ISSN 0965-545X, Polymer Science, Ser. A, 2011, Vol. 53, No. 6, pp. 510–520. © Pleiades Publishing, Ltd., 2011.
Original Russian Text © K.L. Levin, N.S. Pshchelko, 2011, published in Vysokomolekulyarnye Soedineniya, Ser. A, 2011, Vol. 53, No. 6, pp. 906–917.

Electrochemical Properties of a Polypyrrole–Polyimide Composite

K. L. Levin[a] and N. S. Pshchelko[b]

[a] *Institute of Macromolecular Compounds, Russian Academy of Sciences, Bol'shoi pr. 31, St. Petersburg, 199004 Russia*
[b] *St. Petersburg State Mining University, Dvadtsat' Pervaya liniya 2, St. Petersburg, 199106 Russia*
e-mail: levinkl@hotmail.com

Received June 9, 2010;
Revised Manuscript Received January 24, 2011

Abstract—The electrochemical properties of a polypyrrole–polyimide composite are studied from the point of view of its prospective use as a material in polymer-based charge-storage devices, that is, rechargeable batteries and supercapacitors. The content of polypyrrole and the polarization potential of the composite are varied in the experiments. The charge behavior of the composite is characterized via potential step amperometry and electrochemical impedance spectroscopy. The results are discussed in terms of various physical models that take into account the formation of charge-transfer complexes and the storage of electric energy in the double electric layer. A relationship is found between the type of doping (cationic or anionic) of the matrix and the filler and the origin of the charge-storage ability: the capacity due to doping or energy storage in the double electric layer.

DOI: 10.1134/S0965545X11060083

INTRODUCTION

Conjugated polymers (CPs) constitute a new class of organic materials with unique electrical properties, such as high electric conductivity (up to 10^4 S/cm for doped polyacetylene [1]), high electric activity [2], the ability to form inert layers on metal surfaces [3, 4], and a band structure characteristic of semiconductors [5]. These properties are of particular interest in terms of the practical use of CPs [6]. The most promising domains of application of CPs are electromagnetic-radiation shields [7], antistatic coatings [8], polymer-based rechargeable batteries and supercapacitors [9, 10], corrosion-protection coatings [11], and light-emitting devices [5].

Polypyrrole (PPy), polythiophene, polyfuran, polyaniline (PANI), and polyacetylene (PAc) have been study the most and are the most appropriate candidates for practical applications.

Aromatic polyimides (PIs) were first mentioned in the patent literature in the mid-1960s [12]. These polymers are very attractive for conductive composites owning to their excellent thermal stability, very good mechanical properties, and high environmental tolerance [6]. Therefore, CP–PI composites are of considerable practical interest. In this study, we used PI based on poly(pyromellitic dianhydride-*co*-4,4'-oxydianiline), which is known in Russian industry as PM, as a matrix for a composite with CPs. Another advantage of PI as a matrix for composites with CPs in terms of charge-storage ability is its electric activity, i.e., the ability of a film deposited on the electrode to change its degree of oxidation or reduction during immersion into a solution containing electrolyte ions and under an applied electric potential.

Composites that comprise CP as a filler and PI as a matrix have better mechanical properties, chemical stability, and electric conductivity in a wide temperature range than individual CPs have. For example, the temperature at which high electric conductivity in air is preserved is 523 K for PPy and 453 K for PANI [13]. The thermal stability of the PPy–PI composite under the same conditions is above 600 K. A significant improvement in electric conductivity was found for the PANI–PPy composite (550 K) [14]. Composites of this type are used in gas-separation membranes [15–17]. It was proposed to use PPy–PI composites in electromagnetic-radiation shields and antistatic coatings [6, 18–20], rechargeable batteries [21], and gas-separation membranes [22–24]. In addition, these composites exhibit high thermal stability [25].

The relatively high electric conductivity and charge-storage ability of CPs make it possible to use them in supercapacitors and polymer-based batteries [9, 26–28]. Their use in lithium batteries is the most promising, and has been the subject of many recent publications. In particular, it was shown that PPy films easily switch between the anionic and cationic states [29]. A high charge-storage density was revealed for PPy films. The difficulty consisted in choosing an appropriate material to be in contact with the cathode and anode materials [29].

In addition, it is promising to use CPs as active materials in electrochemical supercapacitors [30]. A thin (less than 100 μm) film of a conductive polymer with a high surface area was electrochemically grown on an electrode, which served as a current collector.

During electrochemical formation, the electrode material can be doped in order to obtain either *p*- or *n*-type conductivity. When the electrode is charged or discharged, the dopant ions move between the polymer and the interelectrode gap, while remaining within the double electric layer formed in the pores of the developed surface of the conductive polymer. Thus, in addition to the capacitance of the double electric layer, a pseudo-capacitance results from the electrochemical process. Hence, the specific capacitance of the material (capacitance per gram of weight) can assume extremely high values (up to 400–500 F/g). The charge-storage approach that involves a condenser based on the double electric layer as a positive electrode and a doped polymer as a negative electrode is called a hybrid approach and is described in the literature [31, 32].

The aim of this study is to find the mechanisms of interaction between the matrix and the filler in the PPy–PI composite, which are of practical interest for understanding the composite's electrochemical behavior.

EXPERIMENTAL

Reagents

In the experiments, the poly(amic acid) (PAA) of poly(pyromellitic dianhydride-*co*-4,4'-oxydianiline) was used (DuPont; the Russian counterpart is PM). The test solution of the provider was a 25% solution of PAA in *N*-methylpyrrolidone. All other reagents were purchased from Aldrich.

Sample Preparation

Preparation of a PAA film on the surface of stainless steel. Plates of 410S stainless steel were treated with 600-grit sandpaper and degreased via placing in hexane for 5–10 s. PAA was diluted tenfold with DMAA and stirred at 50°C for 2 h. The resulting diluted solution was applied on the plate surfaces at an amount necessary for the formation of a thick film with a thickness of 15–20 μm (~0.5 cm^3 of solution per cm^2 of plate) and dried at 60°C for 2 h. The prepared plates were used no later than 12 h after drying.

Imidization of PAA. Imidization (conversion of PAA to PI) was performed chemically in a solution that contained pyridine and acetic anhydride [33] and was monitored spectroscopically [34].

Preparation of samples with PPy. The electrochemical deposition of PPy on the stainless steel plates was performed in a single-chamber electrochemical cell in a solution that contained 0.01 M pyrrole and 0.1 M potassium hexafluorophosphate (KPF_6) in acetonitrile. A Princeton Applied Research 273A potentiostat/galvanostat was employed to maintain the electrochemical parameters. The electrochemical cell consisted of a working electrode and a stainless steel counter electrode. A saturated calomel electrode was used as a reference electrode. Hereinafter, unless otherwise stated, all potentials are given relative to the saturated calomel electrode. Electropolymerization was performed at a direct current with a density of 1 mA/cm^2. The circuit opened after passage of a required quantity of electricity. Because of the anodic free-radical electrochemical polymerization, the working electrode was coated with a black PPy film that adhered to the electrode surface. After electrodeposition, the plates with the PPy coating were washed in acetonitrile for 10 min and stored in a desiccator.

The amount of PPy, m (g), derived via electropolymerization was calculated from the formula

$$m = Fk_{el}Q, \quad (1)$$

where F is the Faraday constant, 96 485 C/mol; k_{el} is the electrochemical reaction coefficient (g mol/C^2); and Q is the passed charge (C).

The experimentally determined value of Fk_{el} was 6.2×10^{-3} g/C.

Preparation of PPy–PI composite samples. To prepare the PPy–PI composite samples, PPy was electrpolymerized on an electrode precoated with a PI film. After preparation of the composite, the samples were washed in ethanol and stored in a dry desiccator.

ANALYTICAL PROCEDURES

Scanning electron microscopy. Scanning electron microscopy was performed with a Hitachi S-4000 instrument. The studied surfaces were sputtered with gold.

Potential step amperometry. The charge–discharge properties were studied via potential step amperometry. In the experiments, the film was charged at constant potential E_{ch} for time t_1. After that, the potentiostat was switched to discharge potential E_{dch}; discharge current I was registered as a function of time t_2. The measurements were performed on the electrode surface without and with coatings of PI, PPy, and PPy–PI at different charge times and potentials. To perform this experiment in situ, the same electrochemical cell in which the films were synthesized was used without removal of the working electrode. Prior to potential step amperometry, the derived PPy films were subjected to electrochemical dedoping. For this purpose, the solution in the cell was replaced with 0.1 M KPF_6 in acetonitrile. The dedoping was performed via bridging of the working electrode and the counter electrode for 5 min. The dedoping was monitored according to the discharge current of the film, which decreased from a few milliamperes to picoamperes after dedoping for ~2.5 min. During dedoping, the dopant ions were released from the PPy film into the solution, a phenomenon that was accompanied by a flow of electrons to the external circuit. After dedoping, the film was charged. The value of E_{ch} was selected

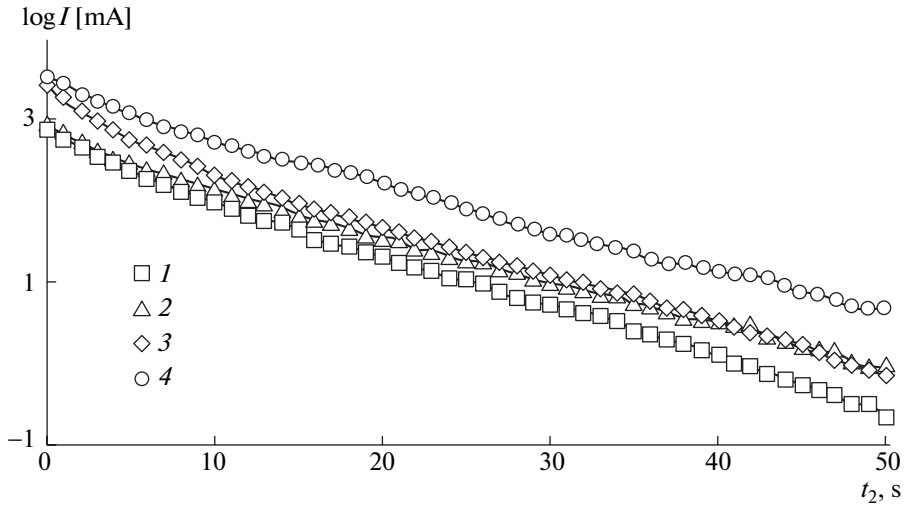

Fig. 1. Dependence of discharge current on discharge time for different charge times t_1 of PPy on the stainless-steel electrode: E_{ch} = 1.1 V; 0.01 M KPF_6 in acetonitrile; 1 mA/cm^2; 500 s; t = (*1*) 10, (*2*) 20, (*3*) 40, and (*4*) 80 s.

in the range 0.5–2.1 V; E_{dch} = 0 V. The quantity of electricity supplied by the film to the external circuit during discharge was calculated from the area under the curve $I = I(t_2)$. For this experiment, a Princeton Applied Research 273A potentiostat/galvanostat was used.

The RC time constant was determined from the slope of the log current–time curve.

Electrochemical impedance spectroscopy. Electrochemical impedance spectroscopy was performed with a Gamry Series G 750 potentiostat. For the experiments, a single-chamber electrochemical cell, which is a typical cylindrical glass tube with a bulge for attachment to the sample with a metal clamp, was used. During electrochemical impedance measurements, the sample coated with the studied film was used as a working electrode. The electrochemical cell was screened from electromagnetic interference by a grounded metal grid. The experiments were conducted in the frequency range 10^{-2}–10^5 Hz.

The impedance of the cell, r_{cell}, was found from the Bode plot under the assumption that it is equal to the scalar impedance at a frequency of $1/2\pi$ Hz.

RESULTS AND DISCUSSION

Charge–Discharge Properties of Various Types of Films

The charge–discharge processes were studied via potential step amperometry; first, the electrode was charged and, then, the discharge curve was measured. These processes are associated with the energy storage–output in the double electric layer at the stainless-steel/electrolyte interface under an applied potential. The discharge curves of PI on the stainless-steel electrode were nonlinear. The discharge current on the electrode coated with PI was ~2 orders of magnitude greater than that on the uncoated electrode (10^{-2} to 10^{-5} A/cm^2 without the coating and $10^{0.5}$ to $10^{-1.5}$ A/cm^2 with the coating for 0–40 s of discharge). Apparently, this result was due to the mobile π-electron system of a molecule that can move relative to the backbone of the molecule and thus contribute to the energy storage by the electric field.

The discharge behavior of PPy significantly differed from that of PI. The discharge-current–discharge-duration curves (hereinafter, discharge curves) for different charge times t_1 are shown in Fig. 1. The discharge current value achieved 10 mA/cm^2. This value is 2–2.5 orders of magnitude higher than that for the PI film, a result that probably is due to both the combined (electrochemical and capacitive) contribution of PPy in comparison with the purely capacitive contribution of PI and the different nature of the capacitive contribution to PI and PPy. To distinguish between the capacitance phenomena in the double electrical layer and the electrochemical effects, let us introduce the concepts of "ultracapacitance" C_{ul} and "pseudo-capacitance" C_{ps}. Total capacitance C_{tot} is

$$C_{tot} = C_{ul} + C_{ps}. \quad (2)$$

The discharge curves of PPy remained approximately linear throughout the discharge (Fig. 1). In terms of the equivalent electric circuit, this is a purely capacitive behavior because it can be characterized by the simplest *RC* circuit, whereas high values of discharge currents, in contrast, seemed to indicate a significant contribution of dedoping. The composite film showed the presence of two successive discharge modes in the same plot (Fig. 2); the first undoubtedly referred to dedoping. At the beginning of discharge, dedoping maintained a discharge with a potential decreasing according to the nonlinear relationship on the chosen scale. After some time characterized by the presence of a step in the discharge curve, the curve became linear.

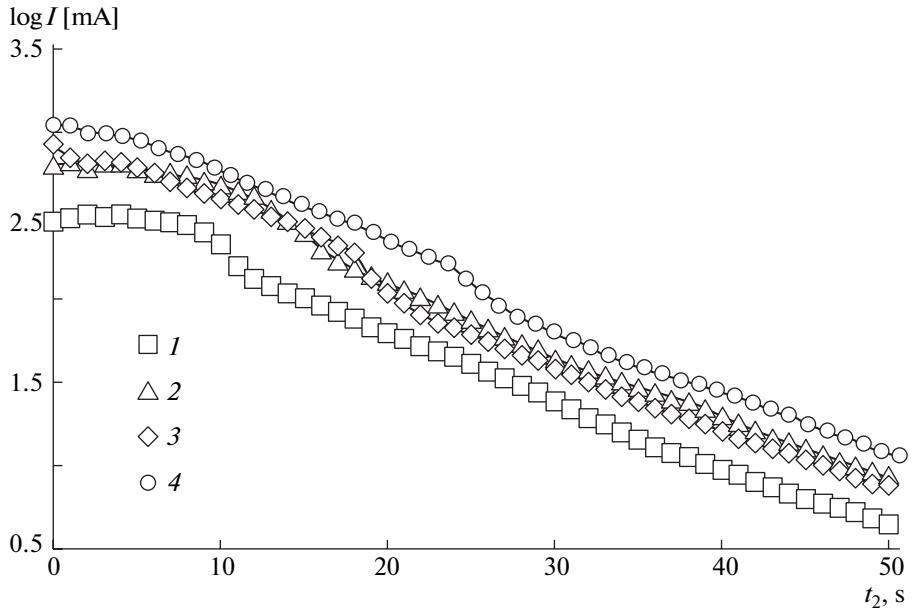

Fig. 2. Dependence of discharge current on discharge time for different charge times (t_1) of the PPy–PI composite on the stainless-steel electrode: E_{ch} = 1.1 V, 0.01 M KPF_6 in acetonitrile, 1 mA/cm^2, 500 s.

The equivalent electric circuit of the dedoping control mode is depicted in Fig. 3. It contains an electrochemical battery, which is responsible for the dedoping, in-parallel with the capacitor. The electric charge that can be stored by the polymer film is an important characteristic of the film. The value of this charge depends on the charging potential. The dependence of the electric charge released by the film to the external circuit, Q_{dch}, on E_{ch} is shown in Fig. 4. It exhibits an extreme behavior; in addition, the maximum value for the PPy–PI composite is higher than that for PPy.

It is of interest to discuss the effect of the PI matrix on the increase in the electric capacity of the composite in terms of electrochemistry. The electrolyte in the solvent undergoes dissociation:

$$KPF_6 \rightleftarrows K^+ + PF_6^- \quad \text{(I)}$$

Under the applied positive potential, PPy is doped as follows:

$$PP^0 + PF_6^- \overset{E}{\rightleftarrows} PP^+/PF_6^- + e^- \quad \text{(II)}$$

Here, acronym PP^0 denotes a PPy molecule fragment in which a deficit of one electron occurs. The electron in the given reaction either comes to the external circuit and causes electric current or is captured by PI (PI^0),

$$PI^0 + e^- \overset{E}{\rightleftarrows} PI^-, \quad \text{(III)}$$

which, for purposes of electroneutrality, is likewise doped:

$$PI^- + K^+ \rightleftarrows PI^-/K^+ \quad \text{(IV)}$$

Owning to the specific structure of this PI molecule, the charge delocalization between monomer units is absent and one negative charge falls within one monomer unit. The exchange reaction with the release of the dopant, a reaction that does not contribute to current either, can occur, i.e.,

$$PP^+/PF_6^- + PI^-/K^+ \rightleftarrows PP^+/PI^- + K^+ + PF_6^-, \quad \text{(V)}$$

as is shown in the following scheme.

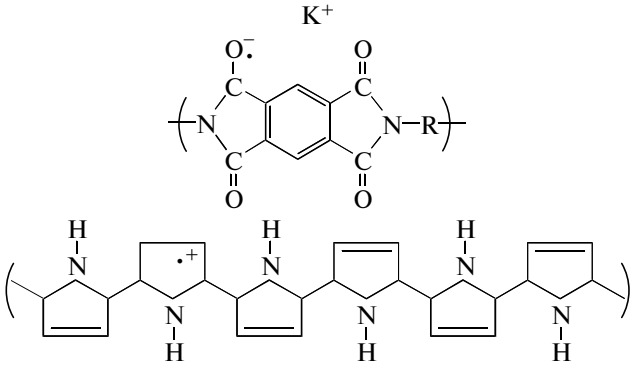

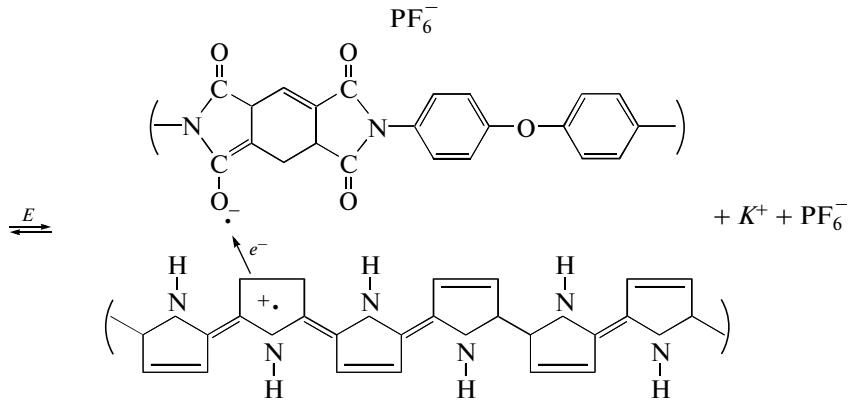

The formation of complexes in reaction (V) was confirmed spectroscopically [35]. It is evident that the formation of the PPy–PI complex as such, in contrast to what was previously thought, did not lead to an increase in the contribution to pseudo-capacitance, because no gain in the number of electrons was observed in the composite. Moreover, the electron released on the right-hand side of (II) can be absorbed into the left-hand side of (III). Nevertheless, the charge-storage ability of the composite significantly increases relative to that of the pure PPy (Fig. 4). This difference may be explained by a higher degree of doping of PPy with dopant ions in the composite due to the role of the PI matrix's prevention of air oxidation of PPy, by improvement of the contact with the electrode due to adhesion, and by the enhanced contribution from the ultracapacitance. The results of impedance measurements (see below) show that precisely this contribution is principal.

Use of the Composite for Corrosion Protection

An increase in the potential of the working electrode above a certain value led to the release of gas bubbles at the composite/electrode interface and to the delamination of the film from the electrode. At high anode potentials, in the gap between the film and the electrode, oxygen anions were oxidized owing to the presence of trace amounts of water in solution according to the reaction

$$2(H^+OH^-) \rightarrow O_2\uparrow + 4H^+ + 4e^-$$

Similarly, hydrogen cations were reduced on the cathode:

$$2e^- + 2(H^+OH^-) \rightarrow H_2\uparrow + 2OH^-$$

The phenomenon of inhibition of CPs in the reduction of molecular oxygen is used in the practice of corrosion protection of metals [36]. The direct refining of the surface with both CPs [36] and nanoadditives that control the corrosion process via single-electron chemical reactions [37, 38] are used for this purpose. The wider the electrochemical stability win-

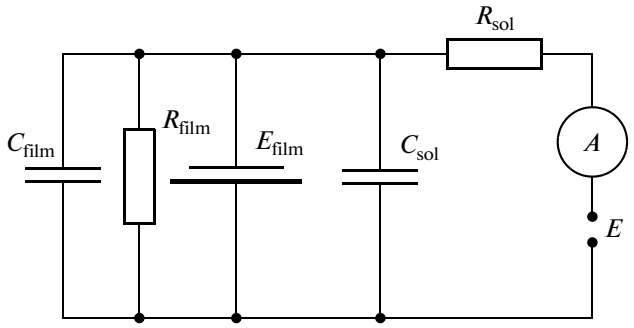

Fig. 3. Equivalent electric circuit: R_{film} is the resistance of the polymer film, E_{film} is the electrochemical potential of the doped polymer film, C_{sol} is the capacitance of the cell and the solution, A is responsible for the control of current, and E is the charging voltage measured with a potentiostat.

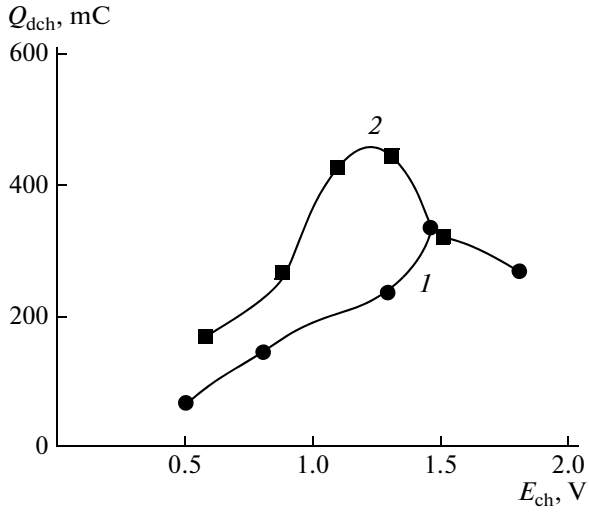

Fig. 4. Dependence of the electric-charge quantity released by the film during discharge, Q_{dch}, on charging potential E_{ch}: (*1*) PPy and (*2*) the PPy–PI composite.

dow of the electrode, i.e., the potentials at which the film does not delaminate, the lower the corrodibility of the electrode. In the presence of PPy, the stability window of the electrode coated with the composite widened by 0.2–0.7 V, a phenomenon that evidently occurred because the film inhibited the electrochemical reactions of water decomposition that lead to corrosion.

Study of the Films via Electrochemical-Impedance Spectroscopy

The total capacitance of the films is composed of the low-frequency C_{lf} and high-frequency C_{hf} components:

$$C_{tot} = C_{hf} + C_{lf} \quad (3)$$

In the absence of polarization at a direct current, electrochemical-impedance spectroscopy makes it possible to derive the component of ultracapacitance from expression (3) through the use of information about the polarization of the PI molecule associated with energy storage in the double electric layer. Since the excitation-pulse amplitude is extremely small (about 0.1 V), in the absence of polarizing potential E_{pol}, no contribution comes from doping and $C_{lf} = 0$ because the doping of PPy occurs at higher positive potentials than 0.6–0.7 V. Thus, with the use of electrochemical-impedance spectroscopy at $E_{pol} = E_{ocp}$ (OCP is the so-called open-circuit potential), it is possible to measure only polarization ultracapacitance.

The convenience of electrochemical-impedance spectroscopy consists in the fact that ultracapacitance can be registered as C_{hf} even when the film is doped and is at certain polarization $E_{pol} \neq E_{ocp}$.

According to the theory of electrochemical-impedance spectroscopy, Nyquist plots can be used to draw conclusions about the presence and structure of the interface. An ideal barrier film on the surface of a conducting electrode looks like a semicircle [39]. In actual practice, the overlap of several semicircles often happens; it is observed as an ellipse or the upper part of an ellipse, an outcome that is indicative of barrier properties. Such was not the case for a pure PI film, whose Nyquist plot was an arc that contained points of the entire frequency range (Fig. 5), thereby signifying the absence of a well-defined interface and the penetration of the solution into the fairly porous PI film.

The equivalent electric circuits corresponding to the electrodes with different coatings are shown in Fig. 6. The circuit of the electrode coated with the PI film included the capacitance of the PI film, C_{PI}; the resistance of the PI film, R_{PI}; and the resistance of the solution, R_s (Fig. 6a). In the presence of PPy, the plot changed. It exhibited the upper part of a semicircle degenerated into the state of a straight line (Fig. 5) as a result of the appearance of an additional interface. In the model shown in Fig. 6b, $R_{PPy/PI}$ denotes resistance of the PPy–PI composite; $C_{PPy/PI}$ is responsible for the appearance of the additional capacitance. The high-frequency semicircle is indicative of the presence of the double electric layer, which apparently formed owing to the appearance of the composite/matrix interface.

Ultracapacitance of PI and PPy Films

The ultracapacitance of the pure PI film was studied via analysis of the Bode and Nyquist plots constructed in the frequency range $0.01–10^5$ Hz under an applied polarization potential in the range from 0 V to delamination. All measurements were performed for two identical samples; one was subjected to anodic polarization until delamination, while the other was subjected to cathodic polarization until delamination. Figure 7a shows that C_{ul} of the pure PI film as a function of positive potential slightly decreases, a result that is probably due to broadening of the double electric layer at the PI/solution interface at positive potentials.

A stepwise increase in capacitance was observed at negative potentials. This process is shown in Fig. 7. At 0.6–0.7 V, the reduction of PI occurred [40]; in addition, the number of $PI^-–PF_6^+$ complexes increased, which led to the increase in ultracapacitance owing to an increase in dielectric permittivity.

The Nyquist plot for the PPy–PI composite as a function of positive potential is depicted in Fig. 8. The plot shows the semicircle degenerated into the upper part, which is preserved in the potential range 0–0.8 V. The capacitance as a function of potential linearly increases at positive potentials. This behavior can be explained by an increase in the number of $PPy^+–PF_6^+$ complexes that is due to the doping of PPy with ions of electrolyte (II), which penetrate into the composite through pores.

At negative potentials, the capacitance of the composite logarithmically increases (Fig. 9). At negative potentials, the macromolecular chain of PI apparently becomes less flexible owing to the orientation of $C=O^-$ groups in the direction of the electric field. In addition, the dielectric permittivity and therefore the polarization capacitance (ultracapacitance) increase. We can try to quantitatively characterize this dependence in the form of the Arrhenius equation:

$$N = n_0 \exp\frac{E - \mu}{kT}, \quad (4)$$

where n_0 is the concentration of units capable of ionization, k is the Boltzmann constant, T is the absolute temperature, and μ is the activation energy for the formation of complexes with PI. The value of μ calculated by taking the logarithm of the curve (Fig. 10) was 0.0728 eV, which almost coincided with the activation energy for the temperature dependence of the electric conductivity of PPy doped with the same dopant in the

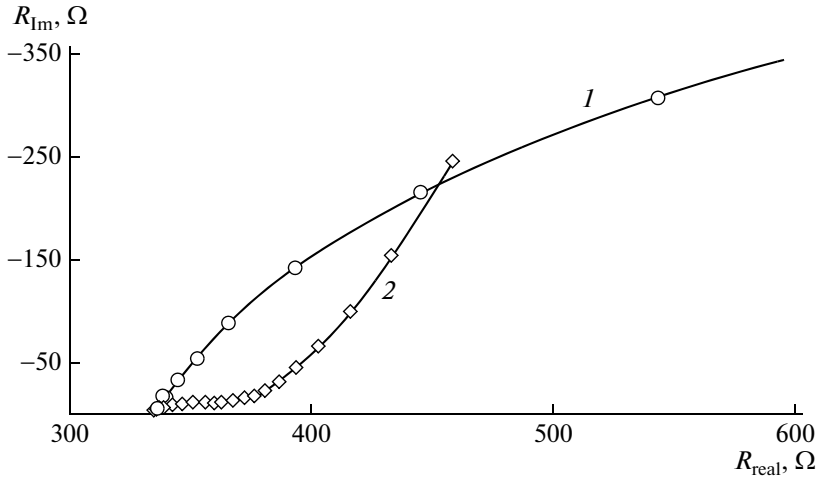

Fig. 5. Nyquist plots for (*1*) the PI film and (*2*) the PPy–PI composite. The concentration of KPF_6 in acetonitrile is 0.01 M; the time of application of PPy is 100 s at 1 mA/cm^2.

range 5–300 K (0.080–0.085 eV) [41]. This result is explained in terms of the model of variable range hopping (VRH) [42], which confirms the correctness of the assumption about the role of free oscillations of ions in the temperature behavior of capacitance.

Ultracapacitance of the Composite

The effect of PPy on the ultracapacitance of the PPy–PI composite was studied via electrochemical impedance spectroscopy as a function of coating thickness, that is, the PPy application time (Fig. 11). The Nyquist plot changed its shape as the amount of PPy increased (Fig. 12). The semicircle shifted to the left owing to an increase in capacitance in the range 8.1 mF/cm (the PPy-free film of PI with a thickness of 20 μm) to 45 mF/cm for the maximum amount of PPy corresponding to a polymerization time of 400 s. This finding indicates that the ultracapacitance greatly increases in the presence of PPy, as shown in Fig. 11.

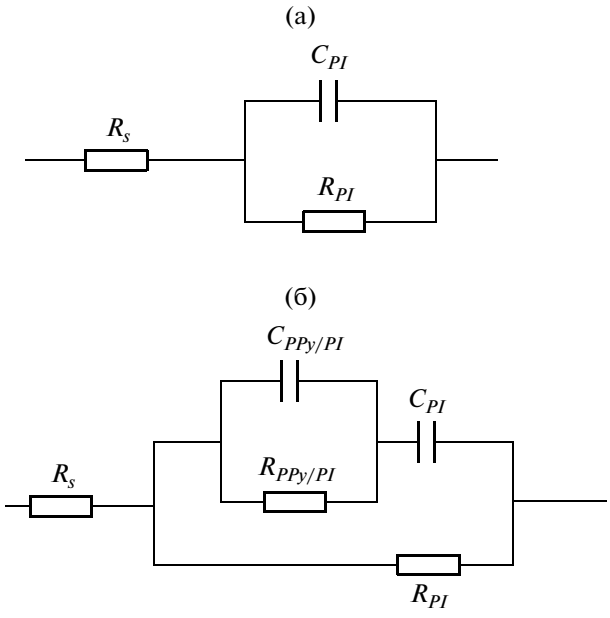

Fig. 6. Equivalent electric circuits that show the impedance properties of stainless-steel electrodes coated with (a) PI and (b) PPy–PI.

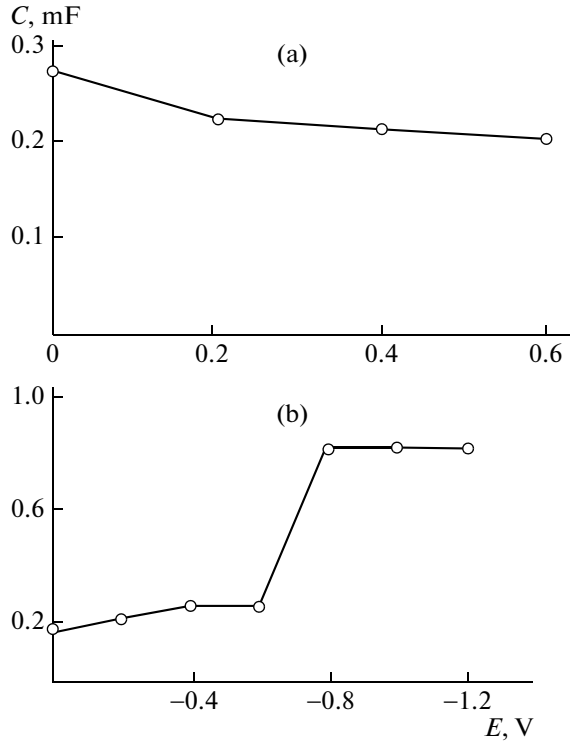

Fig. 7. Capacitance of the PI film as a function of potential: (a) positive potential and (b) negative potential.

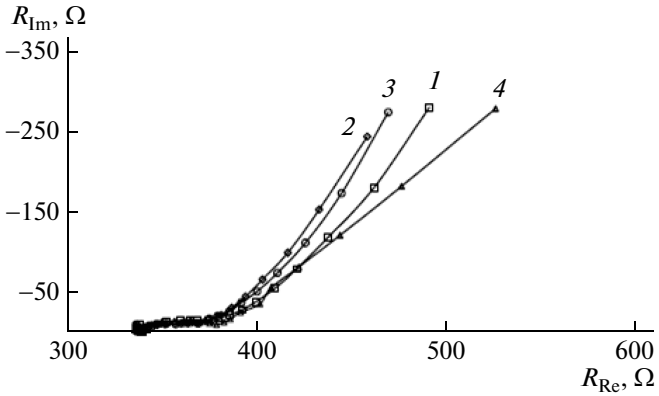

Fig. 8. Nyquist plots of the composite for polarization potentials of (*1*) 0, (*2*) 0.2, (*3*) 0.4, and (*4*) 0.8 V. The time of application of PPy is 100 s at a current density of 1 mA/cm^2.

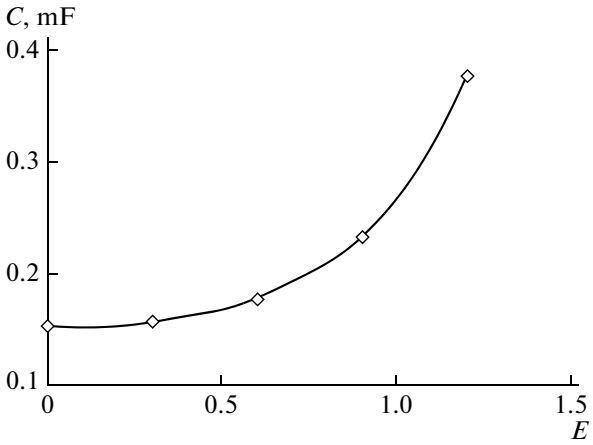

Fig. 9. Capacitance of the PPy–PI composite as a function of negative potential. The time of application of PPy is 100 s at a current density of 1 mA/cm^2. Here and in Fig. 10, the value of E is given relative to saturated calomel electrode.

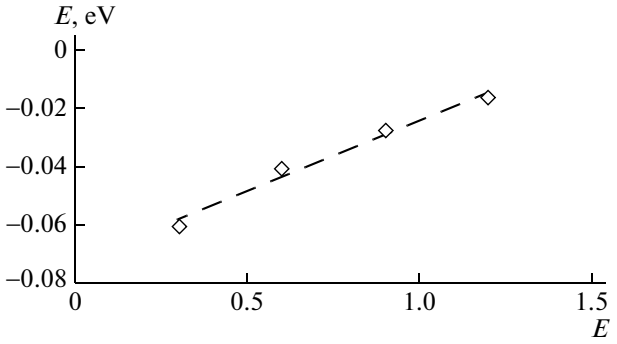

Fig. 10. Activation energy for internal rotations of a PI molecule as a function of the applied potential.

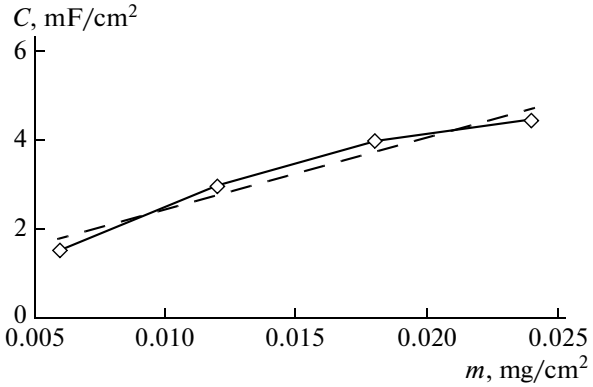

Fig. 11. Capacitance of the PPy–PI composite vs. amount of PPy.

Pore Resistance

If two probes are introduced into a solution, its electric conductivity σ can be measured. On condition that the electric conductivity is induced by ions of several different types *i*, it is

$$\sigma = \sum n_i \mu_i |q_i|, \quad (5)$$

where n_i is the concentration, q_i is the charge, and μ_i is the mobility of the *i*th ion.

A membrane that exhibits resistance to the motion of ions through it can be placed into the gap between the electrodes. If membrane resistance r_{pore} is much higher than solution resistance r_{sol} ($r_{pore} \gg r_{sol}$), the solution resistance measured on both sides of the membrane will actually characterize the membrane pores; therefore, it can be called the pore resistance [43].

If perfectly regular cylindrical pores were being used (Fig. 13a), then the resistance of one individual ideal pore $j_{pore,j}$ would be

$$r_{pore,j} = \rho \frac{d}{A_p} \quad (6)$$

Here, d is the pore length and A_p is the shear area of the pore,

$$A_p = \pi r_{geom}^2, \quad (7)$$

where r_{geom} is the geometric radius of the pore and ρ is the resistivity of the solution in the pore, which is

$$\rho = \sigma^{-1} \quad (8)$$

If pore *j* is not perfectly cylindrical (Fig. 13b), its resistance $r_{pore,j}$.j[ital] is determined from the integral

$$r_{pore,j} = \rho \int_0^d A_p^{-1}(z)dz \quad (9)$$

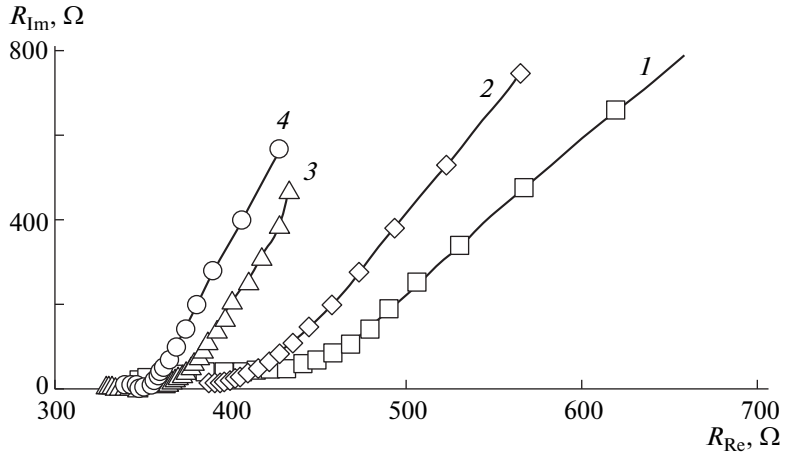

Fig. 12. Nyquist plots of the PPy–PI composites for times of application of PPy of (*1*) 100, (*2*) 200, (*3*) 300, and (*4*) 400 s. $E_{DC} = 0$ V relative to the saturated calomel electrode.

by analogy with expression (6), which is valid for a pore in which cross-sectional area S does not change along length d. In this integral, $A_p(z)$ is the z-coordinate-dependent cross-sectional area of the pore in the direction perpendicular to the vector of z, d is the film thickness, and ρ is the resistivity of the solution in the pore. The origin of coordinates coincides with the bottom face of the film. The pore is assumed to be "regular," that is, a pore in which, for one coordinate z, there is only one projection of the pore cross section onto the z axis. (Self-intersections are absent.) If the resistances of individual pores are summed over j and the rule of parallel-connected resistors is applied, the pore resistance of the entire film can be found:

$$r_{pore}^{-1} = \sum_{i=1}^{N} r_{pore,\,j}^{-1}. \quad (10)$$

Bode plot–derived cell resistance r_{cell} measured at a low frequency ($1/2\pi$ Hz) can be expressed as

$$r_{cell} = r_{sol} + r_{pore} + r_{pol} \quad (11)$$

In this equation, r_{sol} is a solution resistance of ~30 Ω, which is approximately an order of magnitude less than r_{cell} and therefore is disregarded, while r_{pol} is the polarization resistance, which is approximately equal to or greater than r_{pore}. Thus, we can assume that

$$r_{cell} \approx r_{pol} + r_{pore} \quad (12)$$

Dependence of Composite Resistance on the Amount of PPy

As the amount of PPy increased, the value of r_{cell} measured in the absence of potential on the film decreased. Since, in the absence of the potential, we have $r_{pol} = 0$, then

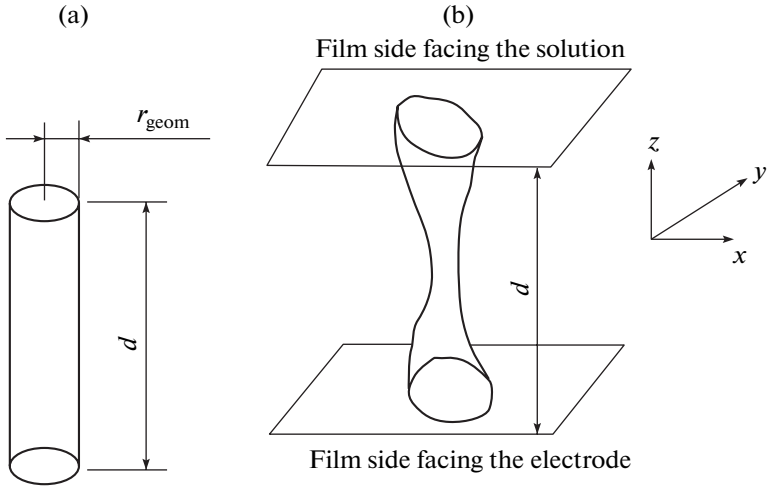

Fig. 13. Images of (a) ideal and (b) nonideal pores.

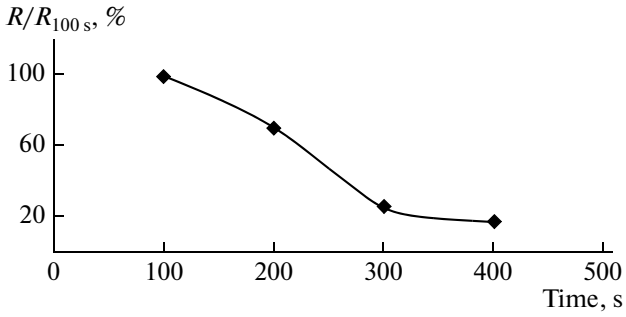

Fig. 14. Relative pore resistance of the PPy–PI composite as a function of PPy content.

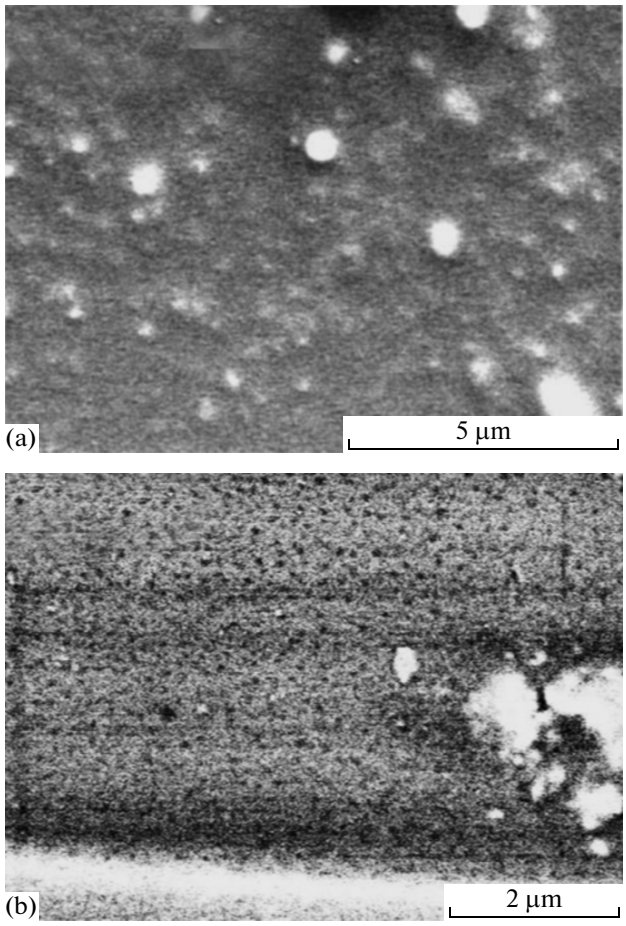

Fig. 15. Structure of the PPy–PI composite for a time of application of PPy of 500 s. The imidization time is 60 min. The top face; magnifications of (a) ×10000 and (b) ×30000.

$$r_{cell} \approx r_{pore} \quad (13)$$

Figure 14 shows that the resistance decreased almost fivefold with a change in the time of application of PPy from 100 to 400 s, a result that can be attributed to an increase in the porosity of the composite film during an increase in the thickness of the coating. The pores that are formed in the composite film during application of PPy are clearly seen from comparison of Figs. 15a and 15b. An increase in pore diameter during an increase in the amount of PPy leads to a decrease in the value of $(A_p)^{-1}$ in expression (9) and, thus, to a decrease in r_{pore}^{-1} in (10).

CONCLUSIONS

The results of the experimental study of the charge–discharge properties of the PPy–PI composite suggest the occurrence of two modes of charge storage: doping–dedoping and control double electric layer. Contrary to what was previously thought, the bare fact that PI is an electroactive polymer decreases, rather than increases, the electric capacitance of the composite in long-term charge–discharge processes related to dedoping (pseudo-capacitance). Thus, ultracapacitance (the capacitance associated with the double electric layer) significantly increases. Therefore, the composite of PPy, which is a "hole" conductor, and PI, which is an "electron" conductor, is more promising for use in supercapacitors than in polymer-based rechargeable batteries. This conclusion can be generalized to any matrix and filler that are prone to exhibiting opposite types of conductivity. In contrast, if the system comprises a similarly doped filler and matrix, the contribution to ultracapacitance will be smaller and the contribution to pseudo-capacitance will be larger.

In our opinion, these results are of interest for the design of hybrid charge-storage devices based on conductive polymers, which combine the properties of a capacitor and a battery.

ACKNOWLEDGMENTS

We thank V.I. Frolov (Institute of Macromolecular Compounds, Russian Academy of Sciences), Dr. Jude Iroh (University of Cincinnati, United States), and Dr. Dennis Tallman (University of North Dakota, United States) and all our other colleagues for their assistance, for useful discussions, and for sharing their experience.

REFERENCES

1. H. Shirakava, E. J. Louis, A. G. MacDiarmid, et al., J. Chem. Soc, Chem. Commun., 578 (1977).
2. *Handbook of Conducting Polymers*, Ed. by T. A. Scotheim, R. L. Elsenbaumer, and J. R. Reynolds (Marcel Dekker, New York, 1998).
3. K. Shah, Y. Zhu, J. O. Iroh, and O. Popoola, Surf. Eng. **17**, 20012 (2001).
4. J. O. Iroh and R. Rajagopalan, Surf. Eng. **16**, 321 (2000).
5. R. Sivaraman, S. J. Clarson, B. K. Lee, et al., Appl. Phys. Lett. **77**, 328 (2000).

6. Yu. N. Sazanov, Zh. Prikl. Khim. (S.-Peterburg) **74**, 1253 (2001).
7. A. Kaynak, Mater. Res. Bull. **31**, 845 (1996).
8. R. S. Kohlman and A. J. Epstein, in *Handbook of Conducting Polymers*, Ed. by T. A. Scotheim, R. L. Elsenbaumer, and J. R. Reynolds (Marcel Dekker, New York, 1998), p. 92.
9. T. F. Otero and I. Cantero, J. Power Sources **81–82**, 838 (1999).
10. S. Panero, P. Prosperi, F. Bonino, and B. Scrosati, Electrochim. Acta **32**, 1107 (1987).
11. J. O. Iroh and W. Su, J. Appl. Polym. Sci. **71**, 2075 (1999).
12. G. Endry, US Patent No. 3,179,630.
13. *Handbook of Conducting Polymers*, Ed. by T. A. Scotheim (Marcel Dekker, New York, 1980).
14. H. Moon, G. Im, and S. Soon, J. Appl. Polym. Sci. **67**, 1863 (1998).
15. T. M. Su, I. J. Ball, J. A. Conklin, et al., Synth. Met. **84**, 801 (1997).
16. H. Yanagasita, D. Kitamoto, K. Haraya, et al., J. Membr. Sci. **135**, 121 (1997).
17. G. A. Polotskaya, T. A. Kostereva, and G. K. Elyashevich, Sep. Purif. Technol. **14**, 13 (1998).
18. K. L. Levin, V. N. Zgonnik, and V. I. Frolov, Polymer Science, Ser. B **35**, (1993) [Vysokomol. Soedin., Ser. B **35**, 1702 (1993)].
19. B. Tieke and W. Gabriel, Polymer **31**, 20 (1990).
20. F. Selampinar, U. Akbulut, and L. Toppare, Synth. Met. **84**, 185 (1997).
21. W. Lu, X. S. Meng, and Z. Y. Wang, J. Polym. Sci., Part A: Polym. Chem. **37**, 4295 (1999).
22. T. M. Su, I. J. Ball, J. A. Conklin, et al., Synth. Met. **84**, 801 (1997).
23. H. Yanagasita, D. Kitamoto, K. Haraya, et al., J. Membr. Sci. **135**, 121 (1997).
24. G. A. Polotskaya, T. A. Kostereva, and G. K. Elyashevich, Sep. Purif. Technol. **14**, 13 (1998).
25. K. L. Levin, T. I. Borisova, V. N. Zgonnik, et al., Polymer Science, Ser. B **42**, @ (2000) [Vysokomol. Soedin., Ser. B **42**, 357 (2000)].
26. M. Satoh, H. Ishikava, K. Amano, et al., Synth. Met. **71**, 2259 (1995).
27. C. Arbizzani, M. Mastragostino, and L. Meneghello, Electrochim. Acta **41**, 21 (1996).
28. S. Panero, P. Prosperi, F. Bonino, and B. Scrosati, Electrochim. Acta **32**, 1107 (1987).
29. M. Hepel, Electrochim. Acta **41**, 63 (1996).
30. X. Ren, J. Davey, A. Rudge, et al., in *Proceedings of Second International Seminar on Double-Layer Capacitors and Similar Energy Storage Devices, Deerfield Beach, 1992.*
31. F. Croce, S. Sacchetti, and B. Scrosati, J. Power Sources **162**, 685 (2006).
32. P. Novak, F. Joho, M. Lanz, et al., J. Power Sources **97–98**, 39 (2001).
33. M. M. Koton, V. V. Kudryavtsev, V. A. Zubkov, et al., Vysokomol. Soedin., Ser. A **26**, 2584 (1984).
34. M. I. Bessonov, M. M. Koton, V. V. Kudryavtsev, and L. A. Laius, *Polyimides: A Class of Thermostable Polymers* (Nauka, Leningrad, 1983) [in Russian].
35. J. O. Iroh and K. L. Levine, Eur. Polym. J. **38**, 1547 (2002).
36. K. L. Levine, D. E. Tallman, and G. P. Bierwagen, ECS Trans. **1** (4), 81 (2005).
37. M. Kendig, M. Hon, and L. Warren, Prog. Org. Coat. **47**, 183 (2003).
38. D. E. Tallman, K. L. Levine, C. Siripirom, et al., Appl. Surf. Sci. **254**, 5452 (2008).
39. M. J. Ross, *Impedance Spectroscopy: Emphasizing Solid Materials and Systems* (Wiley, New York, 1987).
40. R. C. Haushalter and L. J. Krause, Thin Solid Films **102**, 161 (1983).
41. K. L. Levine and A. N. Ionov, in *Proceedings of GSGA Students Research Meeting, Cincinnati, 2002.*
42. N. F. Mott and E. A. Davis, *Electronic Properties in Non-Crystalline Materials* (Clarendon, Oxford, 1971).
43. K. Levine and J. Iroh, J. Por. Mater. **11**, 87 (2004).

Spell: OK